NASA/TM—2000–210200

A Review of Electrical Impedance Spectrometry Methods for Parametric Estimation of Physiologic Fluid Volumes

(MSFC Center Director's Discretionary Fund Final Report, Project No. 96–03)

B. Dewberry
Marshall Space Flight Center, Marshall Space Flight Center, Alabama

January 2000

The NASA STI Program Office...in Profile

Since its founding, NASA has been dedicated to the advancement of aeronautics and space science. The NASA Scientific and Technical Information (STI) Program Office plays a key part in helping NASA maintain this important role.

The NASA STI Program Office is operated by Langley Research Center, the lead center for NASA's scientific and technical information. The NASA STI Program Office provides access to the NASA STI Database, the largest collection of aeronautical and space science STI in the world. The Program Office is also NASA's institutional mechanism for disseminating the results of its research and development activities. These results are published by NASA in the NASA STI Report Series, which includes the following report types:

- TECHNICAL PUBLICATION. Reports of completed research or a major significant phase of research that present the results of NASA programs and include extensive data or theoretical analysis. Includes compilations of significant scientific and technical data and information deemed to be of continuing reference value. NASA's counterpart of peer-reviewed formal professional papers but has less stringent limitations on manuscript length and extent of graphic presentations.

- TECHNICAL MEMORANDUM. Scientific and technical findings that are preliminary or of specialized interest, e.g., quick release reports, working papers, and bibliographies that contain minimal annotation. Does not contain extensive analysis.

- CONTRACTOR REPORT. Scientific and technical findings by NASA-sponsored contractors and grantees.

- CONFERENCE PUBLICATION. Collected papers from scientific and technical conferences, symposia, seminars, or other meetings sponsored or cosponsored by NASA.

- SPECIAL PUBLICATION. Scientific, technical, or historical information from NASA programs, projects, and mission, often concerned with subjects having substantial public interest.

- TECHNICAL TRANSLATION. English-language translations of foreign scientific and technical material pertinent to NASA's mission.

Specialized services that complement the STI Program Office's diverse offerings include creating custom thesauri, building customized databases, organizing and publishing research results...even providing videos.

For more information about the NASA STI Program Office, see the following:

- Access the NASA STI Program Home Page at ***http://www.sti.nasa.gov***

- E-mail your question via the Internet to help@sti.nasa.gov

- Fax your question to the NASA Access Help Desk at (301) 621–0134

- Telephone the NASA Access Help Desk at (301) 621–0390

- Write to:
  NASA Access Help Desk
  NASA Center for AeroSpace Information
  7121 Standard Drive
  Hanover, MD 21076–1320

NASA/TM—2000–210200

A Review of Electrical Impedance Spectrometry Methods for Parametric Estimation of Physiologic Fluid Volumes

(MSFC Center Director's Discretionary Fund Final Report, Project No. 96–03)

B. Dewberry
Marshall Space Flight Center, Marshall Space Flight Center, Alabama

National Aeronautics and
Space Administration

Marshall Space Flight Center • MSFC, Alabama 35812

January 2000

Available from:

NASA Center for AeroSpace Information
7121 Standard Drive
Hanover, MD 21076–1320
(301) 621–0390

National Technical Information Service
5285 Port Royal Road
Springfield, VA 22161
(703) 487–4650

TABLE OF CONTENTS

LIST OF FIGURES

LIST OF ACRONYMS

AC	alternating current
ADC	analog-to-digital converter
BIA	bioimpedance analysis
BIS	bioimpedance spectrometry
BPM	beats per minute
DAC	digital-to-analog converter
DC	direct current
DSP	digital signal processor
ECG	electrocardiogram
ECW	extracellular water
EIS	electrical impedance spectrometry
EMI	electrical interference
FFM	fat-free mass
HDT	head-down tilt
ICW	intracellular water
MFBIA	multiple-frequency bioimpedance analysis
PROM	programmable read-only memory
rms	root mean square
SNR	signal-to-noise ratio
SRAM	static random access memory
TBW	total body water

NOMENCLATURE

A	cross-sectional area
α	a variable to incorporate the distribution of time constants
C_m	membrane capacitance
j	$\sqrt{-1}$
L	segment length
μ	mean
ρ	specific resistivity
σ	standard deviation
R	lumped resistance
r	correlation coefficient
R_c	resistance at the characteristic frequency
R_e	extracellular resistance
R_{ecw}	resistance of extracellular water
R_i	intracellular resistance
R_{icw}	resistance of intracellular water
R_∞	resistance at infinite frequency
R_0	resistance at a frequency of zero (DC)
s	relaxation time constant of dielectric suspension
τ	system time constant
τ_0	mean time constant of the time-constant distribution

NOMENCLATURE (continued)

ω_c	characteristic frequency
Y	function of admittance
Z^*	complex impedance loci
Z_0	impedance at zero frequency (DC)
Z_∞	impedance at infinite frequency
Z_L	load impedance

TECHNICAL MEMORANDUM

A REVIEW OF ELECTRICAL IMPEDANCE SPECTROMETRY METHODS FOR PARAMETRIC ESTIMATION OF PHYSIOLOGIC FLUID VOLUMES (MSFC Center Director's Discretionary Fund Final Report, Project No. 96–03)

1. INTRODUCTION

When an astronaut enters microgravity, he or she experiences a general shift of body fluids toward the head. The lack of a continual, downward gravitational force causes a redistribution of the extra stores of fluid in the calves and thighs toward the head and neck which may result in discomfort and edema. Over a number of days, the body adapts by eliminating excess fluids and limiting fluid intake until achieving a new equilibrium of fluid volumes. A very similar phenomenon occurs during extended bed rest on the ground. And just as one may feel lightheaded or faint when standing up after extended bed rest, an astronaut can experience this loss of consciousness (syncope) upon returning to the Earth or landing on Mars, where his or her health and performance is most critical. Accurate, real-time measurement of these physiologic fluid shifts allows more extensive modeling and analysis of this component of "space adaptation syndrome" and its countermeasures.

A certain amount of fluid volume information can be gained through the application of electrical impedance spectrometry (EIS) with parameter estimation algorithms. This report documents a small effort at Marshall Space Flight Center to test the use of EIS techniques to estimate intercompartmental and intersegmental fluid shifts in a human calf. Previous studies of fluid shifts in space and during bed rest are reviewed, the theory and mathematical models of tissue conductivity are explained, and a description of the development and testing of EIS hardware and software are provided.

2. BACKGROUND

2.1 Fluid Shifts During Space Flight and Bed Rest Studies

Flight experiments conducted on *Skylab*, Spacelab, and Soviet missions have indicated that soft tissue fluids which on Earth pool in the vasculature and interstitium of the legs exhibit a redistribution to the head and chest in microgravity due to removal of the hydrostatic gravitational gradient.[1] Leg volume, measured by plethysmograph and calf girth measurements on a number of Shuttle missions, exhibited an initial exponential decrease of 1.5–2 L in the leg depending on overall weight with a time constant of 6–10 hr and overall settling time of 3–5 days.[2]

Fluid movement (as opposed to loss of muscle, bone, or fat mass) accounts for nearly all of the volume change due to the rapidity of the loss upon entering microgravity and the quick return of fluid volume after landing. After the initial fluid shift, a general fluid loss accompanied by decreased fluid intake causes a typical decrease in total body water (TBW) of 1.7 to 3 percent within 2 days after launch.[1] These changes in body fluid volume and distribution are suspected to be a fundamental cause of subsequent cardiovascular system changes which occur during brief (2–11 days) Shuttle flights.[3]

Similar fluid shifts occur during postural changes on the ground. Early investigations, including that of Hargens et al.,[4] showed that head-down tilt (HDT) elicits physiologic responses quite similar to those of space flight. Hargens et al. tracked qualitative and quantitative measures on eight subjects before, after, and during 8 hr of to 5° HDT. Decreased leg volume (–3.2 percent calf circumference, –4.5 percent leg volume by water displacement), increased urine output, facial edema, nasal congestion, headache, and orthostatic intolorance from HDT are very similar to responses in actual weightlessness. This study in particular indicated a transcapillary fluid shift by measuring sharp decreases in interstitial fluid pressures in both the muscle (4.6 to –2.8 mmHg) and subcutaneous tissues (0.6 to –3.8 mmHg) during HDT.

2.2 Standard Countermeasures to Fluid Shifts

The standard test for the cardiovascular fitness of Shuttle astronauts (as well as ground-based bed rest subjects) is the "passive stand test" in which the heart rate and blood pressure is measured during 5 min of supine rest followed by 5 min of standing upright. Preflight (normal), the heart rate increases from ≈57 to ≈70 beats per minute (BPM), leveling off after 2–3 min. Postflight measurements, after a flight of 2–8 days, reveal that the initital supine heart rate begins higher—as high or higher than the preflight standing rate. Upon standing, the postflight heart rate jumps to >100 BPM and continues to increase for the duration of the test.[3] Syncope can result.

The standard Shuttle countermeasure to this "space adaptation syndrome" as it is sometimes called, is oral rehydration with 32 oz of liquids and eight salt tablets beginning ≈1 hr before returning to Earth. Called "fluid loading," this countermeasure decreases the postflight supine heart rate as well as the increase in postflight supine and standing heart rates, but it does not eliminate the continued increase

in postflight standing heart rate which continues for the duration of the test. In addition, the effectiveness of oral rehydration on heart rate decreases with an increase in time spent in microgravity until, after flights of ≥10 day, there seems to be no differences between users and nonusers of this countermeasure.[3]

These results indicate that more than one process may be at work. Short-term orthostatic hypotension may be caused by loss of total body fluids, including a decrease in total plasma volume of 12 percent,[5] while longer term adaptations include increased venous compliance[6] with a modification of the setpoint for intravascular control.[7]

2.3 Computer Modeling

Questions remain involving the fundamental processes which drive these responses. What causes a decrease in total plasma volume? Does a decrease in total volume cause increased venous compliance? How could fluid shifts result in modifications of the baroreceptor reflex? The last question has been greatly researched and debated. Early investigators proposed that a suppression of antidiuretic hormone due to an increase in central venous pressure caused by a large fluid shift from lower to upper body segments may cause the fluid loss and reflex changes.[8] The problem is that central venous pressure does not seem to increase at all. Studies from Spacelab 1 and ground-based simulations could not find an increase in central venous pressure either during spaceflight or in the launch posture.[3]

A few researchers have attempted to apply a version of Guyton's overall fluid, electrolyte, and cardiovascular system regulation model to the problem.[9,10] Simanonok et al.[11] have modified the model to include the gravitational vector direction and magnitude as a variable to support planning and interpretation of HDT studies. Simulation results, which match those from flight data from Spacelab Life Sciences–1, propose a mechanism for the decrease in fluid volumes to a low point in ≈8 day followed by some recovery. The model includes a complex cascade of events which could cause cardiovascular and fluid regulation changes experienced on orbit. The model indicates that a decrease in hematocrit and protein concentration over days with a quick fluid shift and total volume decrease over hours can be the cause of the undershoot in blood volume which achieves a minimum at about day 3 followed by some recovery. The model is used to postulate mechanisms which can focus experimentation and instrumentation.

Likewise, the same group has published results which use the same computer program to model the effectiveness of lypressin to extend the effects of fluid loading to increase antidiuresis.[12] They favorably compared actual and simulated urine volumes during HDT and made some adjustments to model the dosage effects of lypressin. The model successfully predicts a 50-percent less decrease in fluid volume after 4 hr using lypressin and fluid loading as a countermeasure compared to using salt and fluid loading alone.

The availability of an accurate systemic model of fluid balance and cardiovascular regulation should be invaluable for keeping track of the various mechanisms involved, and guiding experimental hypothesis and instrumentation selection. Conceivably, all combinations of countermeasures (exercise, lower body negative pressure, fluid loading, antidiuretics, and others) could be applied to the model in combination at many possible stages in adaptation from launch to touchdown. These simulation results could be used to determine the most promising protocols for more expensive and time-critical HDT and space-based experimentation.

However, to be used effectively, any complex model requires accurate measurement of fundamental parameters and calibration of boundary conditions during simulation. Without periodic calibration, phenomena that are measured over time scales of hours can be modeled accurately, while longer term, or weekly time scale, phenomena are at best qualitative. Accurate and fast measurements of intracellular and extracellular fluid volume changes in multiple body segments provide fundamental parameters to an extended cardiovascular system model. Measurement of these data with near continuous resolution extends the usefulness of a cardiovascular system model to provide accurate process dynamics and guide experimentation over a number of days or weeks rather than over short-term hydrostatic HDT studies.

EIS with parameter identification shows promise in filling this role while being noninvasive and portable so that long-duration fluid volume dynamics can be compared in ground and flight studies. To justify this statement, the background of this measurement technique is reviewed, beginning with its basis in volume-conductor theory, continuing through its use in TBW estimation using single and multiple frequencies, and concluding in the state-of-the-art fitting of the impedance spectrogram to the Cole-Cole model of cells in suspension to estimate intracellular and extracellular fluid volumes.

2.4 Simple Volume Conductor Theory of Electrical Impedance Measurement

The adult male human body averages ≈57-percent water, 40 L by weight distributed between intracellular, interstitial, and intravascular compartments. Roughly 25 of the 40 L are intracellular fluid, separated from the other compartments by somewhat leaky cell membranes; 12 L are interstitial, separated from the remaining 3 L of intravascular volume by the vascular walls.[13] These fluids contain sodium, potassium, chloride, and phosphate ions, forming a good electrical conductor.

When a voltage is applied across a cylindrical conductor filled with ions in suspension, these fluids conduct an electric current. The resistivity of this conductor is inversely proportional to the number of charges per unit volume. Ions have conductivities which depend on relative concentrations, mobility, and chemical charge—their ionic strength.[14] Together the various ionic strengths produce a specific resistivity, ρ, for the conductor. As depicted in figure 1, the resistance of a cylindrical body segment with a constant distributed specific resistivity can be determined from its resistivity, length, and cross-sectional area.

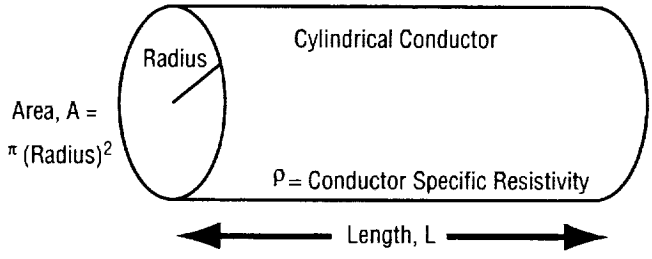

Figure 1. Simplified volume conductor model of segmental impedance.

As Nyboer[15] explains, a lumped-parameter model of segmental resistance can be estimated as

$$R = \rho \frac{L}{A} , \tag{1}$$

where R is the lumped resistance in ohms (Ω), ρ is the specific resistivity in ohm-cm, L is the segment length in cm, and A is the cross-sectional area in cm^2. An electromotive force applied across the length of a homogeneous conductive cylinder produces an evenly distributed electric current within the conductor. The voltage difference measured at any two points along the length of the conductor is proportional to the current passing through the conductor and the resistance of the section between the voltage measurements.

Substituting the geometric calculation of conductor volume $V = L \times A$ and algebraically rearranging provides the relationship for segmental fluid volume in terms of known or measurable quantities

$$V = \frac{\rho L^2}{R} . \tag{2}$$

If resistivity ρ and length L between points of applied potential remain constant, then volume can be determined from measurement of resistance. Alternatively, a resistance measurement which changes over time can indicate a change in fluid volume.

2.5 Clinical Measurement of Total Body Water Using Electrical Impedance

Many researchers have measured whole-body impedance at a single frequency and correlated the inverse of this value to independent measurements of TBW or fat-free mass (FFM). Single-frequency TBW measurement techniques were validated as early as 1969 by Hoffer et al.[16] Later research involved updating and reverifying the technique for clinical use.[17–19]

Hoffer et al.[16] correlated the whole body impedance magnitude and TBW of 20 normals, and used the results to estimate TBW in 34 patients of various clinical disease states. Whole-body impedance was measured using four surface electrodes on the right hand and left foot, imposing a 0.1 mA_{rms} (root mean square) current at 100 kHz through the outer electrodes, and measuring the resulting voltage across the inner electrodes. This measurement, along with height, weight, and wrist circumference were correlated with TBW determined by the tritiated water method with blood samples drawn after 5 and 6 hr for equilibration of the isotope. They found the best relationship was TBW versus the ratio of height (Ht) in meters squared divided by impedance (Ht^2/Z) which had a correlation coefficient, r, of 0.92. Determination and correlation of Ht^2/Z with an ionic mass measurement produced no evident improvement. Using the model determined on the 20 normals (estimated $TBW = A \times Ht^2/Z + B$, where A and B are constants determined by regression on the 20 normals), the TBW of the 34 diseased patients (with renal failure, Cushing's syndrome, or obesity) were estimated with r=0.93.

An important analysis by Hoffer et al. involved the choice of measurement frequency. They measured whole-body impedance magnitude at 0.1, 1, 10, and 100 kHz and showed a fairly rapid

decrease in impedance magnitude from 10–100 kHz. This decrease is apparently due to an increase in conduction via intracellular fluids because of capacitive coupling across cell membranes and they therefore decided to use only the data from 100 kHz (the highest frequency in the data available) in the analysis. However, later research shows that this decrease in impedance magnitude continues to just over 1 MHz,[14] indicating that a better measurement of TBW, intracellular plus extracellular, may be more accurately measured at frequencies ≥1 MHz.

The value of a measurement of TBW alone by these researchers lies in the relationship of TBW, along with age, gender, height, and weight, to lean body, or FFM, a clinical measurement of considerable importance. However, FFM is more closely related to intracellular water (ICW).[20] Therefore, TBW, while useful for normal subjects, produces invalid results when the extracellular-to-intracellular water ratio (ECW/ICW) is not normal. The ECW/ICW ratio is a fundamental component of ρ which is assumed to be a known constant. If this value is unknown (as in diseased subjects) or changing (as in acute HDT studies), it must be measured for accurate results. A number of researchers are investigating multiple-frequency bioimpedance analysis (MFBIA), which, as described in the next section, allows estimation of the ECW/ICW ratio and therefore more general and accurate measurements of TBW, ICW, and FFM.[21,22]

2.6 Intracellular and Extracellular Fluid Impedances

Cell walls are made of lipid bilayers which act as imperfect insulators to an electric current. Any insulator bounded by conductors in an electric field develops opposing charges across the membranes, forming a dielectric with a characteristic capacitance and charging rate. As depicted in figure 2a, this capacitive effect causes an oscillating current source through the length of tissue to follow a path around cells at low frequencies. At higher frequencies, the cell wall capacitances act more as a short, allowing a more straight-line movement of current through the total fluid space.[23]

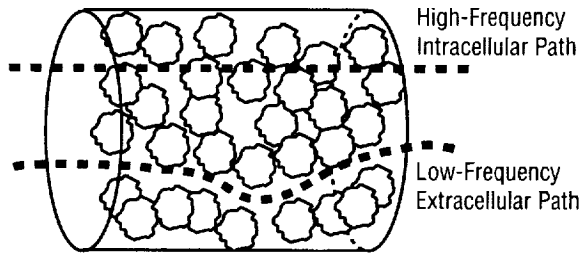

Figure 2a. Simplified body segment illustrating high-frequency and low-frequency current paths.

Figure 2b depicts these paths as an electrical circuit model. Low-frequency current is blocked by the membrane capacitance from entering the intracellular fluid, thus it encounters only extracellular resistance, R_e. Alternating current (AC) with sufficient high-frequency alternatively charges and discharges the membrane dielectric, allowing current to flow through the cell, encountering intracellular resistance, R_i, and R_e.

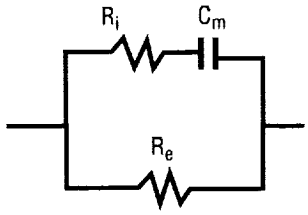

Figure 2b. Equivalent electrical circuit model of electrical conductive path through a body segment.

The electrical impedance encountered by a high-frequency oscillating current is small compared one with low frequency. The reactance due to membrane capacitance, C_m, at high frequencies can be neglected compared to R_i and R_e. Thus the resulting high-frequency impedance equals two resistances in parallel with a phase angle near zero.[14] Mathematically this frequency-dependent resistance, or impedance, is a function of frequency, implying that volume is frequency dependent as well

$$V(\omega) = \frac{\rho L^2}{Z(\omega)} \ , \tag{3}$$

where the impedance $Z(\omega)$ can be derived from the equivalent circuit in figure 3

$$Z(\omega) = \frac{R_e(1 + j\omega C_m R_i)}{1 + j\omega C_m(R_i + R_e)} \ , \tag{4}$$

which can be broken into real and imaginary components

$$Z(\omega) = R(\omega) + jX(\omega) \ , \tag{5}$$

where the real component $R(\omega)$ is

$$R(\omega) = \frac{R_e\left(1 + \omega^2 C_m^2 R_i(R_i + R_e)\right)}{1 + \omega^2 C_m^2(R_i + R_e)^2} \tag{6}$$

and the imaginary componenet $X(\omega)$ is

$$X(\omega) = \frac{-\omega C_m R_e^2}{1 + \omega^2 C_m^2(R_i + R_e)^2} \tag{7}$$

and can be represented in polar form

$$Z(\omega) = |Z(\omega)| + \phi\{Z(\omega)\} \tag{8}$$

with magnitude $|Z(\omega)|$ and phase $\phi\{Z(\omega)\}$ characteristics which are functions of frequency.

A plot of this complex equation is presented in two forms in figure 3(a) and 3(b). Figure 3(a) contains a polar plot with the resistance verses absolute value of the reactance. Figure 3(b) is a Bode plot of approximately the same data. Reactance *(X)* versus resistance R is plotted for varying frequencies. R_0 is the resistance at a frequency of zero and R_∞ is the resistance at infinite frequency. ω_c is the characteristic frequency which equals $1/2pR_iC_m$ for the current in figure 2b.

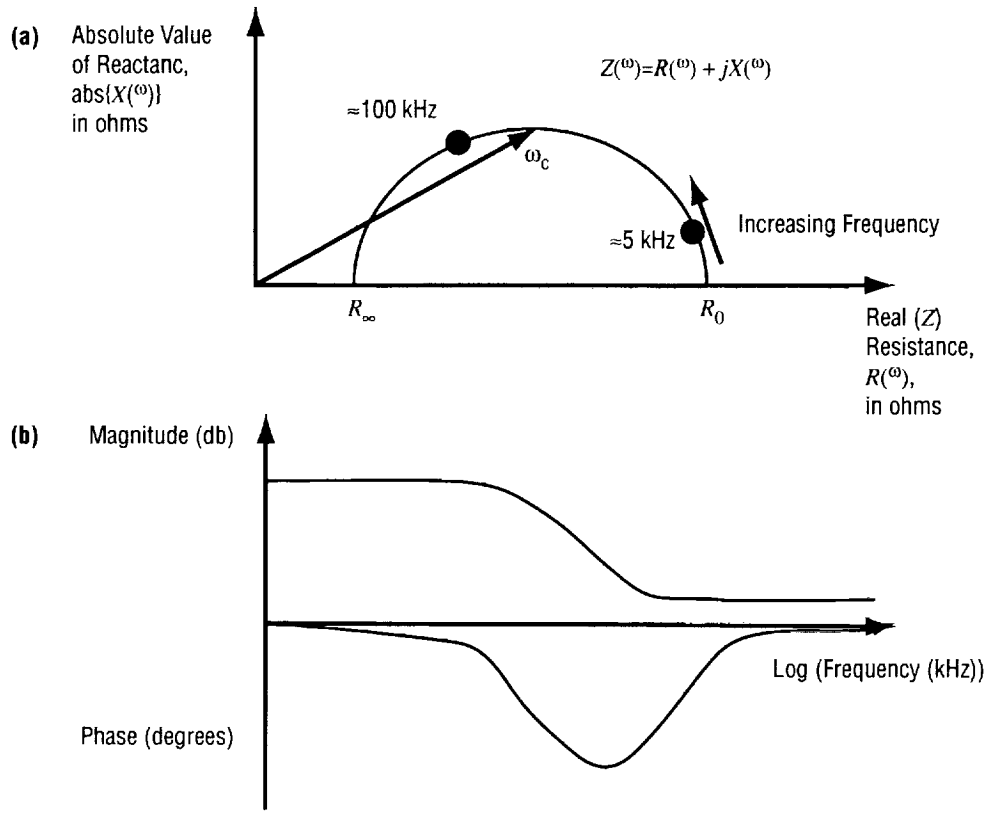

Figure 3. Complex plot of equivalent circuit.

In the polar plot of figure 3(a), {Real($Z(\omega)$, Imag{$Z(\omega)$} are plotted as frequency ω varies from zero to infinity, producing a semicircle which crosses the real axis at two points with a maximum reactance at frequency ω_0. At frequencies <5 kHz, the extracellular resistance, R_e, of the tissue dominates and the impedance has a large magnitude (and real component) and small phase (and imaginary component). As the measurement frequency increases, cell membrane capacitance, C_m, increases the reactance, decreasing the total magnitude and increasing the phase lag. The locus has an apex at a characteristic frequency, ω_c, (≈50 kHz for most muscle tissue, 2 MHz for whole blood), at which the reactive component is maximized. Above the characteristic frequency, the impedance magnitude and phase angle decreases until at very high frequencies the reactance is negligible, resulting in an equivalent circuit of parallel resistances R_e and R_i.[24]

2.7 The Advantages of Multiple Frequency (Spectroscopy) Measurement

The simple equivalent circuit of figure 2b has been used by many investigators to determine intracellular and extracellular impedances. A few researchers measure whole-body impedance at a number of frequencies (2 to 6) between 5–100 kHz, generate the polar plot and visually fit a circle to the data.[20,22] Using this procedure to determine R_0, R_∞, and ω_c; R_e, R_i, and C_m of the equivalent circuit in figure 2(b) can be determined using the identities:

$$R_e = R_0 \tag{9}$$

$$R_\infty = \frac{R_i R_e}{R_i + R_e} \tag{10}$$

and

$$f_c = \frac{1}{2\pi\tau} \quad , \tag{11}$$

where τ = system time constant = $R_i C_m$.

However, actual measurements of impedance spectra have been shown to contain a phenomenon called "depressed loci."[14,23,25] This phenomenon, attributed to the cellular inhomogeneity of the tissue being measured, is thought to be due to a distribution of time constants, known as β dispersion. As depicted in figure 4(a), a tissue with two distinct time constants or electrical relaxation times (possibly

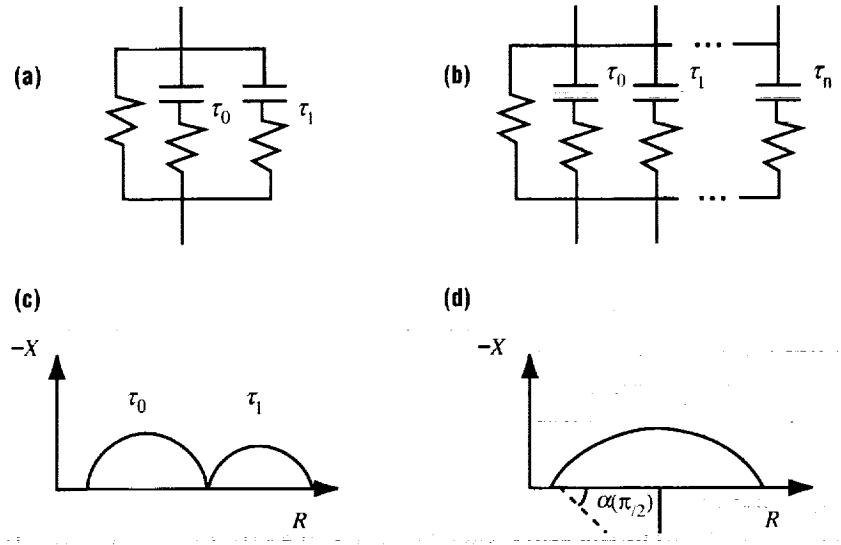

Figure 4. Equivalent circuit model and complex impedance locus for a system with two time constants (a) and (c), and a system with a distribution of n time constraints (b) and (d). A distribution of time constants causes a "depressed" impedance locus.

due to two cell sizes, internal ionic strengths, and/or membrane thicknesses) has two "humps" in the modified polar plot. As the number and dispersion of time constants increases (fig. 4(b)), the distribution of humps effectively produces a circular section locus whose center is depressed below the real axis.

The frequency-domain transfer function is based on admittance rather than impedance. Cole and Cole first derived a frequency-domain transfer function for modeling dielectric fluids.[25] Their basic formula is

$$Z^* - Z_\infty = \frac{Z_0 - Z_\infty}{1 + (j\omega\tau_0)^{1-\alpha}} \ , \tag{12}$$

where Z_∞ is the impedance at infinite frequency, Z_0 is the impedance at 0 frequency (i.e., direct current (DC), j *is* $\sqrt{-1}$, and Z^* is the complex impedance locus based on polar coordinates with origin at Z_∞. The variable α, $0 < \alpha < 1$, is introduced to incorporate the distribution of time constants. As depicted in figure 4(d), $\alpha(\pi/2)$ is the angle between the resistance axis and a vector from the locus crossing at infinite frequency to the center of a circle whose section makes up the locus. Therefore, greater α produces a more depressed locus. An α equaling zero produces a model with one time constant, while an α of 1 effectively produces a system with infinite dispersion and a flat locus. Dimensionless, α typically increases from 0.15 to 0.20 in the human calf when the subject changes from sitting to supine, indicating an increase in the dispersion of cell size and/or internal resistivity.[26]

Kanai et al.[23] expressed the Cole-Cole model as a function of admittance, Y:

$$Y(\omega) = \frac{1}{R_e} + \frac{1}{R_i} - \frac{\frac{1}{R_i}}{1 + (j\omega\tau_0)^{(1-\alpha)}} \ , \tag{13}$$

where τ_0 is the mean time constant of the time-constant distribution. The time-constant distribution is related to the Kanai equation through:

$$Y(\omega) = \frac{1}{R_e} + \frac{1}{R_i} - \frac{1}{R_i}\int_0^\infty \frac{F(\tau)}{1 + j\omega\tau} d\tau \ , \tag{14}$$

where $F(\tau)$ is the Cole-Cole distribution function

$$F(\tau) = \frac{1}{2\pi} \frac{\sin(\alpha\pi)}{\cosh\left((1-\alpha)\log \tau/\tau_0\right) - \cos(\alpha\pi)} \ . \tag{15}$$

This shows that although the distribution function for the time constants would be a normal distribution if the effective characteristics are statistically distributed, Cole and Cole found the more suitable distribution function of eq. (15) through actual measurements of dielectrics in suspension.[25]

Figure 5 graphically compares these two dispersion functions:

(a) Logarithmic Gaussian distribution: $N(s) = \frac{1}{\sqrt{2\pi\sigma^2}} e^{\frac{-(s-\mu)^2}{2\sigma^2}}$

(b) Cole-Cole distribution: $F(s) = \frac{1}{2\pi} \frac{\sin(\alpha\pi)}{\cosh((1-\alpha)s) - \cos(\alpha\pi)}$

Where s is the relaxation time constant of the dielectric in suspension, μ the mean, and σ is the standard deviation.

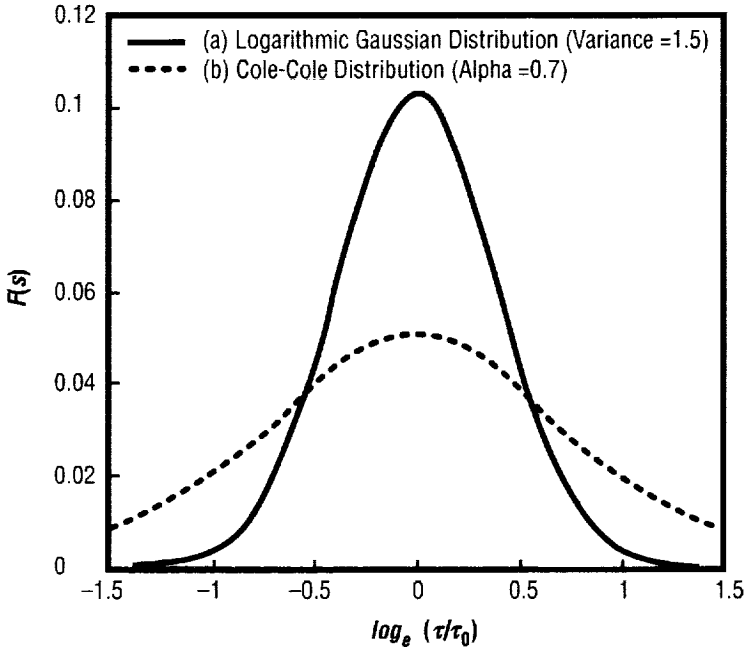

Figure 5. Distribution of relaxation times $F(s)$, where $s=\log_e(\tau/\tau_0)$ and τ/τ_0 is the normalized relaxation time.

The normal distribution requires a larger concentration of relaxation times for values of close to τ_0.[25] However, this distribution was developed by measurement of dielectric liquids (i.e., ethyl alcohol) and preliminary research shows that combined modification of the variance and gain of the normal distribution can approximate any Cole-Cole distribution with value α. The advantage of the Cole-Cole distribution may be its simpler relation to a frequency-domain transfer function.

2.8 Parameter Identification for Total Body Water Volume Estimation

Use of multiple-frequency impedance measurements with a linear regression fit to the Cole-Cole model is becoming standard practice in current literature. Both whole-body composition investigations and isolated-segment fluid volume analysis have been reported by investigators to improve the accuracy of estimations of fluid volumes by measuring impedance at multiple frequencies and fitting the data to the Cole-Cole model (eq. (12)).

Cornish et al. compared single-frequency impedance methods, or bioimpedance analysis (BIA) with multiple-frequency methods, or bioimpedance spectrometry (BIS).[22] They measured the whole-body impedance magnitude and phase of 42 rats at six frequencies from 1 to 100 kHz and least-squares fit the data to the Cole-Cole equation (eq. (13)). They compared the results to those derived at a single frequency (50 kHz) with independent measures of TBW using deuterium oxide dilution and ECW using isotope [^{3}H]-inulin. The multiple-frequency BIS estimation with least-squares fit to the Cole-Cole parameters was used to determine TBW by estimating the resistance at the characteristic frequency (R_c). This value was not much improved over the single-frequency method (correlation coefficient r=0.965 for BIS versus r=0.950 for BIA). However, the BIS determination of R_0 (impedance magnitude at zero frequency derived from Cole-Cole least squares) was quite accurate (r=0.993), showing that the use of a Cole-Cole derived R_0 improves approximation of R_0 by direct measurement at 5 or 1 kHz.

Similarly, Lichtenbelt et al.[27] compared whole body TBW and ECW measurements using a standard two-frequency technique and multiple-frequency Cole-Cole fitting technique with TBW and ECW measurements and deuterium and bromide-dilution techniques. They found a much smaller (±0.04) standard deviation in ECW measurements when the multiple frequency-derived ratio R_{ecw}/R_{icw} was included versus the standard deviation (±0.22) from the two-frequency (1 and 100 kHz) technique.

These results tend to support the underlying utility and theory of Cole-Cole for whole-body analysis. However, TBW prediction using a single high-frequency impedance estimate does not show much improvement, perhaps because a single-specific characteristic resistivity ρ for both intracellular and extracellular fluid volumes is implicit in the calculation of R_c, the characteristic impedance magnitude, or R_∞, the extrapolated impedance magnitude at infinite frequency. K. Cole,[28] studying cells in suspension, found that ρ_{ecw} averages 3 to 4 times higher than ρ_{icw}, possibly due to the exquisite control of ionic diffusion exerted by cells.[13] This suggests that a slightly improved model may contain an extracellular resistance which is set at 3 to 4 times higher than that of intracellular resistance.

2.9 Intracellular and Extracellular Volume Measurement in a Single Body Segment

Kanai et al.[23] was the first to report that an impedance spectrum numerically fit against the Cole-Cole model can be used to measure intracellular and extracellular resistance, cell membrane capacitance, and α dispersion in the human calf. No attempt was made, however, to determine fluid volumes, presumably due to inconsistencies in published specific resistivity "constants" ρ of fluids, but instead demonstrated qualitative changes in intracellular and extracellular resistivities before and after exercise.

A few years after Kanai, a group of researchers at Duke University led by Gerth[26] published a description of a system, based on a commercial impedance analyzer, for time-series measurement of impedance with linear regression analysis to the Cole-Cole equation. In a protocol lasting a total of 180 min, they measured the impedance spectrum at 5-min intervals, performing least-squares regression, and plotted Cole-Cole parameters R_i, R_e, C_m, and dispersion coefficient α in the calf and thigh of four human subjects. Gerth and Watke[29] subsequently demonstrated the system by measuring changes in fluid volumes due to diuretics in neurosurgical patients. The instrument requires 70 sec to acquire and analyze the impedance at 50 frequencies between 3 and 150 kHz, producing estimates R_i, R_e, C_m, and

dispersion coefficient α.[29] In addition, Sasser et al.[30] have applied the system in vivo to measure osmotically induced cellular volume changes in the hind-limb of six rats. The data conformed well qualitatively with the theoretic magnitudes and directions of perfusate concentrations which produce changes in cellular volume.

Figure 6 illustrates the results of the calf measurements of one subject from the Gerth et al. study.[26] The subject began in an upright, seated position and at 30 min moved to a supine, 6° HDT posture. This position was maintained for 90 min when they returned to the seated position. No independent measurement of these values was performed for comparison due to the difficulty of otherwise providing measurements of intracellular and total water in an isolated human body segment.

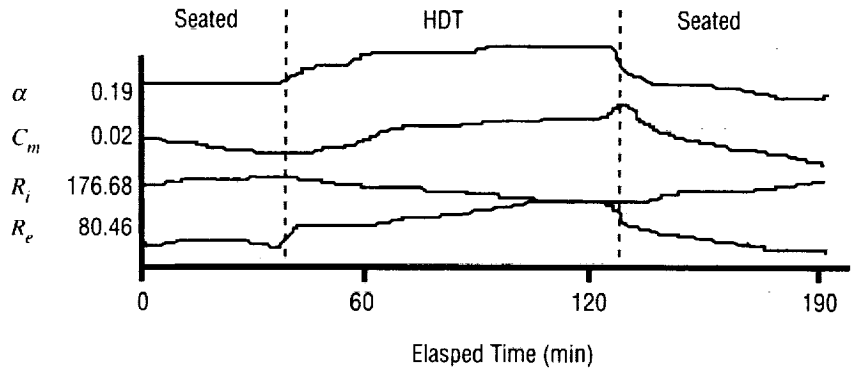

Figure 6. Cole-Cole model parameters over time.

There are a number of interesting phenomena apparent in the plot. Recall from equation (2) that resistance values are inversely proportional to volumes assuming constant specific resistivity. Rapid increases in calf R_e with movement to HDT suggests a rapid emptying of calf vessels as hydrostatic pressures decrease. After about 10 min, this rapid increase in resistance, indicating a rapid decrease in fluid volume, halts when a new intravascular intersegmental hydrostatic balance is achieved. It is replaced with a Starling-mediated slow shift of fluid from interstitial spaces into the vasculature and out-of-the-calf segment. This slow decrease in extracellular volume is mirrored by a decreasing R_i. This, along with the increase in cell membrane capacitance suggests that the calf cells (counterintuitively) enlarged when the subject reclined.

Also interesting are the dynamics of the cellular time-constant dispersion coefficient α. Values of α increase toward 1 indicating a widening of the distribution of tissue time constants. An individual cell's time constant can change due to an increase in R_i or C_m. An increase in α, indicating an increase in standard deviation around an average value, indicates a broadening in the dispersion of cell sizes. Cells closest to capillary membranes may react first and more strongly, with a delay in the propagation of the effects of hydrostatic and osmotic forces through the interstitial gel. Upon return to the seated position, α quickly returns to its smaller value, suggesting that the return of hydrostatic pressure rapidly instigates a return of the cells to uniform size.

These observations are based on the analysis of Gerth's plot of a single subject. Obviously, the validity and sensitivity of the measured parameters must be determined before it becomes the basis for extensive modeling and analysis.

As described, the literature suggests that EIS, BIS, and MFBIA, with subsequent least-squares fit to the Cole-Cole model comprises the state-of-the-art in in vivo fluid measurement using applied electrical potentials. Although application of the Cole-Cole model corrects for an apparent distribution of cell resistivities possibly due to cell size and/or ionic concentration, the theory assumes a perfectly homogeneous suspension of spheroids in a cylinder. More accurate geometric measurements of volumes may produce slight improvements[31] and analysis of the impedance characteristics of specific tissue types[32] have been considered. Uncertainties in intracellular and extracellular resistivities, ρ_{ecw} and ρ_{icw}, make it difficult to measure absolute fluid volumes, but changes in intracellular and extracellular fluid volumes in specific segments can be measured accurately. In fact, with a sufficient number of data points in a spectrum and a more accurately modeled relation between ionic strengths of various tissues; intracellular, extracellular, and whole-blood volume changes can be measured.

3. INSTRUMENTATION DESIGN CONSIDERATIONS

After providing theoretical and practical reasons for using a four-electrode, or "tetrapolar," instrumentation system, two top-level instrument designs are present. The swept-sinusoid design has the advantage of simply deriving the frequency-domain impulse response in analog hardware. The programmable-wave design is centered around the software of a sigital signal processor (DSP) which provides much more flexibility in designing the stimulus wave and therefore may produce a quicker, more accurate response.

3.1 Rationale for a Tetrapolar System

Ackman[14] reports that early research in bioelectric impedance analysis performed measurements using two electrodes. Current was imposed through the body with the same electrodes used to measure the resulting voltage. While this system has the advantage of simpler design and application, it only gives accurate results when electrode contact impedance is considerably smaller than the tissue impedance to be measured.

Biologic tissue has very low impedance. Calf impedance magnitudes from 3–150 kHz derived from data provided by Gerth[26] have a maximum of 38 Ω. On the other hand, the impedance of electrodes and leads reported by Ackman[14] are variable depending on design and application but can be as high as 58 kΩ. Although the use of electrode gel and driven shields can reduce this impedance, a two-electrode system has an electrode impedance which "swamps" the tissue impedances. A four-electrode apparatus with a constant current source reduces the effects of electrode impedance.

To alleviate this problem, state-of-the-art bioelectrical impedance techniques in the literature use a tetrapolar technique as depicted in figure 7. As reviewed by Avhandling[24] the impedance Z_L is the desired measurement. A constant current is applied through a pair of outer electrodes while the resulting voltage is measured through inner electrodes as depicted in figure 7. Z_1 and Z_2 are undesired electrode and lead impedances in the current source circuit. The effects of these impedances are minimized with a good constant-current source design which maintains the current excitation through the circuit with impedances Z_1, Z_L, and Z_2 throughout the impedance magnitude and frequency ranges of interest.

The voltage E_L across the load Z_L is to be measured, while the voltage E_m is the one actually presented at the input terminals of the instrument due to the effects of stray lead and electrode impedances Z_3 and Z_4. In addition, a measurement impedance Z_m is unavoidable but can be made large by using a high-frequency instrumentation amplifier. The voltage, or electromagnetic force, E_1 across Z_1 is given by

$$E_L = E_m\left(1+\frac{Z_c}{Z_m}\right), \tag{16}$$

therefore if the measurement amplifier impedance Z_m is considerably larger than $Z_c = Z_3+Z_4$ then there is essentially no current flowing through the measurement circuit and the effects of Z_c are minimized.

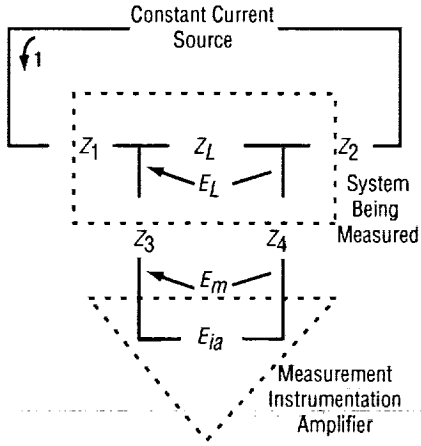

Figure 7. A tetrapolar impedance measuring system with electrode impedances included (adapted from Avhandling (1985)).

3.2 Swept Sine Prototype High-Level Diagram and Description

As depicted in figure 8, a tetrapolar system imposes an oscillating current with constant peak amplitude through the outer electrodes and measures resulting voltage through inner electrodes. Signal conditioning circuitry rectifies and filters the AC voltage producing a DC rms value. The voltage through a constant resistance is rectified and filtered to DC, producing a voltage proportional to current for verification of constant current design. The impedance magnitude is computed as the measured voltage divided by the measured current. The phase difference between the excitation current and measurement voltage is determined by passing the imposed and measured signals through comparators and finding the exclusive-or value of the resulting square waves. The frequency of oscillation is changed and the process continues until an entire impedance spectrum from 1 kHz to 1 MHz is acquired at a number of discrete frequencies.

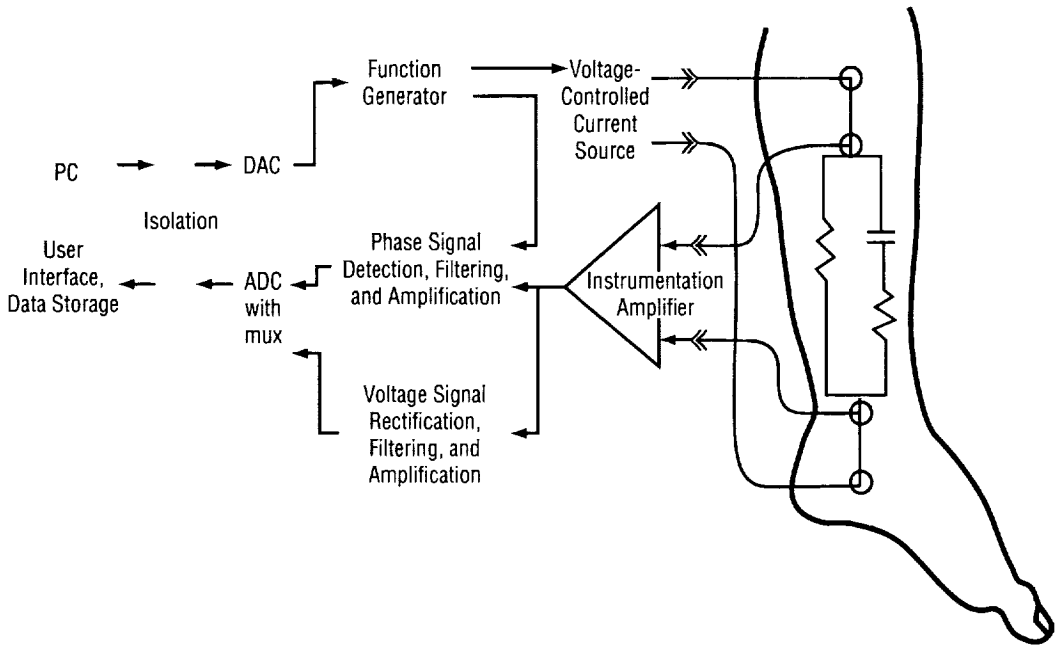

Figure 8. A high-level diagram of a swept sine electrical impedance spectrometer.

4. PATIENT SAFETY CONSIDERATIONS

The most obvious concern with electrical impedance measurements is the susceptibility to electrical shock. After all, EIS involves skin preparation and electrode placement to minimize resistance to current. Fortunately, there are a number of design considerations which can be followed to produce safe and effective electronics.

Olsen[33] describes many unsafe scenarios with design considerations for avoiding these hazards and safety testing procedures. The scenarios include normal operation with incorrect readings, normal operating applied current limits, abnormal macroshocks in any AC-powered electronic equipment, and macroshocks in equipment with patient electrodes.

Normal operation can sometimes be dangerous in critical-care instrumentation if they produce incorrect or hard-to-interpret readings. Examples are electrocardiographs, automatic defillibrators, and respirators. Because the instrument to be developed in this research is to be tested on healthy, normal subjects away from a clinical setting, incorrect readings are not considered dangerous.

Normal operation of an electrical impedance spectrometer imposes a constant peak AC (or as proposed a white-noise current waveform) through the subject. Increasing this current increases the signal-to-noise ratio (SNR) of the instrument. This current is limited by the threshold of perception. According to Olsen, the threshold for perception for a current at 60 Hz is 0.5 mA and the "let-go" current minimum at 60 Hz is 6 mA. Assuming that perception current increases with frequency similar to that of let-go current, a 1,000-Hz signal has a threshold of perception of ≈1 A. The EIS to be developed has a minimum frequency of 1,000 kHz with a maximum amplitude of 5 mA—more than 2 orders of magnitude below the threshold of perception at this frequency.

Gerth[26] used an excitation current amplitude of 0.3 mA at 3 kHz, increased to a maximum of 5 mA at 1 Mhz, allowing maximum SNR and accuracy of measurement at the higher frequencies. The adjustment described by Geddes[34] configures the drive current according to frequency using a log-log relationship $\ln(I) = m\ln(f) + b$; where I is the current at frequency f. Geddes describes safe values of the parameters m and b.

As stated by Olsen, normal operation can cause macroshocks in any electronic equipment connected to AC wall voltage used by and around people. These types of macroshocks occur when someone who is grounded touches a portion of the instrument that is at a high voltage. This is especially hazardous with equipment encased in a metal chassis that is not connected to earth ground. If an internal short occurs between AC voltage and the chassis and a person who is otherwise grounded touches the case, a macroshock condition can occur. This can be prevented by grounding the chassis to earth ground—the third, green conductor in AC plugs. This practice also minimizes the effects of stray electromagnetic interference (EMI). The ground-pin-to-chassis resistance limit is 0.15 Ω throughout the life of the instrument. The chassis-to-ground leakage current should not exceed 100 μA for systems that are likely to contact patients. These tests must be conducted on the instrument before each experiment.

Macroshock prevention is especially important in any medical instrument or procedure which reduces or eliminates the resistance of the skin.[33] Because EIS measurement involves preparing the skin and application of gel electrodes to minimize resistance, it is critical that faults in the internal circuitry not propagate AC line voltages across patient electrodes. This scenario can be avoided by low-voltage operation, electrically isolating the patient leads, and/or battery operation.

The analog electronics of the EIS operate at <15 V, such that even if the feedback in the voltage-controlled current source circuitry fails, the worst that can happen is application of a ±15-V sine wave at 1 kHz. A conservative estimate of electrode and tissue resistance of 500 Ω (preliminary measurements indicate that each electrode provides resistance >1 kΩ) subjects the tissue a maximum current of 3 mA at this frequency. This amplitude and frequency are only of concern as a microshock hazard if one of the electrodes was placed inside or on the surface of the heart.[33]

Olsen states that transformer isolation, optical isolation, or battery operation are the best ways to prevent microshock or macroshock hazards. However, isolation transformers and analog optical isolation amplifiers are typically designed for electrocardiogram (ECG) and other biopotential measurements with maximum frequencies <10 kHz. Imposing these components between the subject and electronic circuitry can cause unacceptable signal attenuation above this frequency. The design goal in this research is to analyze frequencies up to 1 MHz. Transformer and analog optical isolation components with this bandwidth are very expensive or nonexistent. However, very fast digital optical isolation amplifiers are common.

Battery power is a common design choice for external heart pacemakers. Battery power also eliminates measurement noise from 60 Hz power and switching power supplies. However, digital electronics (digital signal processors); static random access memories (SRAM's); and programmable read-only memories (PROM's) in prototypical designs are power hungry and drain all but the largest battery packs in a few hours. A system that uses battery power for analog circuitry with a common AC/DC converter for digital circuitry may be the best compromise. Digital optical isolation amplifiers should be used between the microcontroller, digital-to-analog converter (DAC), and analog-to-digital converter (ADC) to isolate the patient from AC voltages. A high-level schematic design of such a system is given in the appendix.

Such a system passes the patient-lead tests described by Olsen (1978). These include limits of <50 μA in leakage currents measured between each patient lead and earth ground as well as <50 μA leakage currents between any two patient leads. AC isolation is tested by measuring current between the patient leads and hot and neutral AC channels. This current must be <20 μA.

5. SOCIETAL IMPLICATIONS

This research could help humans live and work in space, improve medical diagnosis and treatment of clinical patients on Earth, and improve other biological and materials research. Accurate and real-time measurements of intercompartmental, intersegmental fluid shifts and changes in cellular morphology in astronauts before, during, and after spaceflight could lead to better countermeasures against the disabling orthostatic hypotension which results.[1] On Earth, many people are treated for fluid retention, edema, and kidney failure. Accurate, low-cost, and noninvasive measurement of the time course of compartmental fluid shifts could track improvements during therapy and allow clinicians and researchers to measure real-time pharmaceutical effects of drugs on cell osmolarity and vascular exchange. More accurate and validated EIS with equivalent circuit analysis could improve results in other areas of biology such as seed germination and growth[35], monitoring of grape cells during fermentation, and protein function in cell walls. Nonbiological applications include noninvasive measurement of the structure and degradation of materials, and micro-ohm measurement and process monitoring during annealing of metals and other conductive materials.

APPENDIX—PRELIMINARY DESIGN OF A PROGRAMMABLE-WAVE ELECTRICAL IMPEDANCE SPECTROMETER

Figure 9 shows an example of a programmable-wave electrical impedance spectrometer using a DAC, voltage controlled current source, instrumentation amplifier with gain, anti-aliasing filter, and ADC.

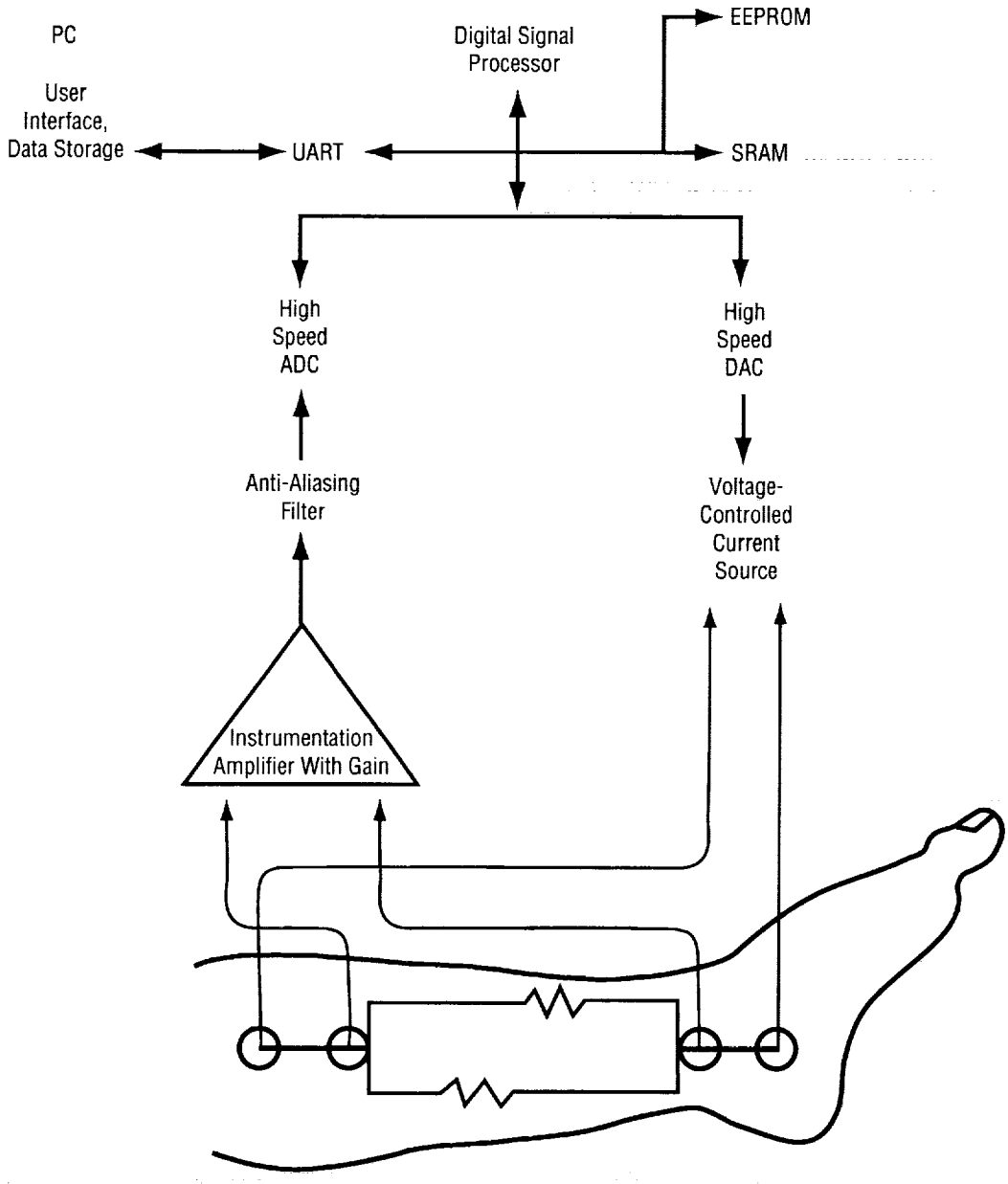

Figure 9. Preliminary design of a programmable-wave electrical impedance spectrometer.

REFERENCES

1. Leach, C.S.; Cintron, N.M.; and Krauhs, J.M.: "Metabolic Changes Observed in Astronauts," *J. Clin. Pharmacol.*, Vol. 31, pp. 921–927, 1991.

2. Nicogossian, A.E.: in *Space Physiology and Medicine*, 2nd ed., A.E. Nicogossian, C.L. Huntoon, and S.L. Pool (eds.), Lea & Febiger, Philadelphia, PA, pp. 139–153, 1989.

3. Charles, J.B.; and Lathers, C.M.: "Cardiovascular Adaptation to Spaceflight," *J. Clin. Pharmacol.*, Vol. 31, pp. 1010–1023, 1991.

4. Hargens R.; et al.: "Fluid Shifts and Muscle Function in Humans During Acute Simulated Weightlessness," *J. Appl Physiol: Respirat. Environ. Exercise Physiol.*, Vol. 54(4), pp. 1003–1009, 1983.

5. Johnson, P.C.: "Fluid Volume Changes Induced by Space Flight," *Acta. Astronaut*, Vol. 6, p. 1335, 1975.

6. Thornton, W.E.; and Rummel, J.A.: in *Biomedical Results from* Skylab, R.S. Johnston and L.F. Dietlein (eds.), NASA SP–377, pp. 191–197, 1977.

7. Gaffney, F.A.; et al.: "The Effects of a 10-day Period of Head-Down Tilt on the Cardiovascular Responses to Intravenous Saline Loading," *Acta. Physiol. Scand.*, Vol. 144, S. 604, pp. 121–130, 1992.

8. Nixon, J.V.; et al.: "Early Cardiovascular Adaptation to Simulated Zero Gravity," *J. Appl. Physiol. Respirat. Environ. Exercise Physiol.*, Vol. 46, pp. 541–548, 1979.

9. Guyton, A.C.; Coleman, T.G.; and Granger, H.J.: "Circulation: Overall Regulation," *Annu. Rev. Physiol.*, Vol. 34, pp. 13–46, 1972.

10. Coleman, T.G.: "Mathematical Analysis of Cardiovascular Function," *IEEE Trans. on Biomedical Engineering*, Vol. BME–32, No. 4, 1985.

11. Simanonok, K.E.; Srinivasan, R.S.; and Charles, J.B.: "Physiologic Mechanisms Effecting Circulatory and Body Fluid Losses in Weightlessness as Shown by Mathematical Modeling," *The Physiologist*, Vol. 36, No. 1, Suppl., pp. 112–113, 1993.

12. Srinivasan, R.S.; et al.: "Simulation of the Fluid Retention Effects of a Vasopressin Analog Using the Guyton Model of Circulation," *The Physiologist*, Vol. 36, No. 1, Suppl., pp. 114–115, 1993.

13. Guyton, A.C.: *Textbook of Medical Physiology*, 8th ed., W.B. Saunders Co., Orlando, FL, pp. 274–275, 1991.

14. Ackman, J.; and Seitz, M.A.: "Methods of Complex Impedance Measurement in Biologic Tissue," *CRC Crit. Rev. Biomed. Eng.*, Vol. 11, pp. 281–311, 1984.

15. Nyboer, J.: *Electrical Impedance Plethysmography; the Electrical Resistive Measure of the Blood Pulse Volume, Peripheral and Central Blood Flow*, 2nd ed., Charles C. Thomas, Springfield, IL, 1970

16. Hoffer, E.C.; Meador, C.K.; and Simpson, D.C.: "Correlation of Whole Body Impedance with Total Body Water," *J. Appl. Physiol.*, Vol. 21. pp. 531–534, 1969.

17. Zarowitz, B.J.; and Pilla, A.M.: "Bioelectrical Impedance in Clinical Practice," *Annals of Pharmacotherapy*, Vol. 23, pp. 548–555, 1989.

18. Khaled, M.A.; et al: "Electrical Impedance in Assessing Human Body Composition: The BIA Method," *Am. J. Clin. Nutr.*, Vol. 47, pp. 789–792, 1988.

19. Lukaski, H.C.; et al.: "Validation of Tetrapolar Bioelectrical Impedance Method to Assess Human Body Composition," *J. Appl. Physiol.*, Vol. 60(4), pp. 1327–1332, 1996.

20. Thomas, B.J.; and Cornish, B.H.: "Bioelectrical Impedance Analysis for Measurement of Body Fluid Volumes: A Review," *J. Clin. Eng.*, Vol. 17(6), pp. 505–510, 1992.

21. Jenin P.; et al.: "Determination of Body Fluid Compartments by Electrical Impedance Measurements," *Aviat. Space Environ. Med.*, Vol. 46(2), pp. 152–155, 1975.

22. Cornish, B.H.; Thomas, B.J.; and Ward, L.C.: "Improved Prediction of Extracellular and Total Body Water Using Impedance Loci Generated by Multiple Frequency Bioelectrical Impedance Analysis," *Phys. Med. Biol.*, Vol. 38, pp. 337–346, 1993.

23. Kanai, H.; Sakamoto, K.; and Haeno, M.: "Electrical Measurement of Fluid Distribution in Human Legs: Estimation of Extra- and Intra-Cellular Fluid Volume," *J. Microwave Power*, Vol. 18(3), pp. 233–243, 1975.

24. Avhandling, A.: "In Vivo Fluid-Volume Monitoring With Impedance Technique," *Masters Thesis*, Kungl Tekniska Hogskolan I., Stockholm, 1985.

25. Cole, K.S.; and Cole, R.H.: "Dispersion and Absorption in Dielectrics. I. Alternating Current Characteristics," *J. Chem. Phys.*, Vol. 9, p. 341, 1941.

26. Gerth, W.A.; Montgomery, L.D.; and Wu, Y.C.: "A Computer-Based Bioelectrical Impedance Spectroscopic System for Noninvasive Assessment of Compartmental Fluid Redistribution," *Proc. Third Annual IEEE Symposium of Computer-Based Medical Systems,* IEEE Computer Society Press, Los Alamitos, CA, pp. 446–453, 1990.

27. Lichtenbelt, W.D.; et al.: "Validation of Bioelectrical-Impedance Measurements as a Method to Estimate Body-Water Compartments," *Am. J. Clin. Nutr.*, Vol. 60, pp 159–166, 1996.

28. Cole, K.S.: *Vol. 1. Membranes, Ions and Impulses: A Chapter of Classical Biophysics*, Univ. of Calif. Press, Berkeley, 1972.

29. Gerth, W.A.; and Watke, C.M.: "Electrical Impedance Spectroscopic Monitoring of Body Compartmental Volume Changes," *J. Clin. Eng.*, Vol. 18(3), pp. 253–60, 1993.

30. Sasser, D.C.; Gerth, W.A.; and Wu, Y.: "Monitoring of Segmental Intra- and Extracellular Volume Changes Using Electrical Impedance Spectroscopy," *J. Appl. Physiol.*, Vol. 74(5), pp. 2180–2187, 1993.

31. Organ, L.W.; et al.: "Segmental Bioelectrical Impedance Analysis: Theory and Application of a New Technique," *J. Appl. Physiol.*, Vol. 77(1), pp. 98–112, 1978.

32. Lu, L.; et al.: "Parametric Modelling for Electrical Impedance Spectroscopy System," *Med. Biol. Eng. Comput.*, Vol. 34, pp. 122–126, 1996.

33. Olsen, W.H.: *Medical Instrumentation: Application and Design*, J.G. Webster, (ed.), Houghton Mifflin, Boston, pp. 667–707, 1978.

34. Geddes, L.A.; et al.: "Hazards in the Use of Low Frequencies for the Measurement of Physiological Events by Impedance," *Med. & Biol. Eng.*, Vol. 7, p. 289, 1969.

35. Ackman J.: "Complex Bioelectric Impedance Measurement System for the Frequency Range from 5 Hz to 1 MHz," *Annals of Biomed. Eng.*,Vol. 21, pp. 135–146, 1993.

REPORT DOCUMENTATION PAGE

Form Approved
OMB No. 0704-0188

1. AGENCY USE ONLY *(Leave Blank)*	2. REPORT DATE	3. REPORT TYPE AND DATES COVERED
	January 2000	Technical Memorandum

4. TITLE AND SUBTITLE
A Review of Electrical Impedance Spectrometry Methods for Parametric Estimation of Physiologic Fluid Volumes
(MSFC Center Director's Discretionary Fund Final Report, Project No. 96–03)

5. FUNDING NUMBERS

6. AUTHORS
B. Dewberry

7. PERFORMING ORGANIZATION NAMES(S) AND ADDRESS(ES)
George C. Marshall Space Flight Center
Marshall Space Flight Center, AL 35812

8. PERFORMING ORGANIZATION REPORT NUMBER
M–978

9. SPONSORING/MONITORING AGENCY NAME(S) AND ADDRESS(ES)
National Aeronautics and Space Administration
Washington, DC 20546–0001

10. SPONSORING/MONITORING AGENCY REPORT NUMBER
NASA/TM—2000–210200

11. SUPPLEMENTARY NOTES
Prepared by Avionics Department, Engineering Directorate

12a. DISTRIBUTION/AVAILABILITY STATEMENT
Unclassified-Unlimited
Subject Category 52
Nonstandard Distribution

12b. DISTRIBUTION CODE

13. ABSTRACT *(Maximum 200 words)*

Electrical impedance spectrometry involves measurement of the complex resistance of a load at multiple frequencies. With this information in the form of impedance magnitude and phase, or resistance and reactance, basic structure or function of the load can be estimated. The "load" targeted for measurement and estimation in this study consisted of the water-bearing tissues of the human calf. It was proposed and verified that by measuring the electrical impedance of the human calf and fitting this data to a model of fluid compartments, the lumped-model volume of intracellular and extracellular spaces could be estimated. By performing this estimation over time, the volume dynamics during application of stimuli which affect the direction of gravity can be viewed. The resulting data can form a basis for further modeling and verification of cardiovascular and compartmental modeling of fluid reactions to microgravity as well as countermeasures to the headward shift of fluid during head-down tilt or spaceflight.

14. SUBJECT TERMS	15. NUMBER OF PAGES
electrical impedance spectrometer, bioimpedance, parameter estimation, volume measurement	36
	16. PRICE CODE A03

17. SECURITY CLASSIFICATION OF REPORT	18. SECURITY CLASSIFICATION OF THIS PAGE	19. SECURITY CLASSIFICATION OF ABSTRACT	20. LIMITATION OF ABSTRACT
Unclassified	Unclassified	Unclassified	Unlimited